Drug Development and Target Identification

INVESTIGATION OF A SERIES OF 1,4-DIARYL-PYRAZOLO-PYRIDINONES AS ANTI-LEISHMANIAL AGENTS

Hannah Corman, Graduate Student, University of Notre Dame

Douglas Shoue, Eck Institute for Global Health, University of Notre Dame

Bruce J Melancon, Vanderbilt University

Mary Ann McDowell, Eck Institute for Global Health, University of Notre Dame

Leishmaniasis is a grouping of diseases caused by the protozoan parasites Leishmania spp., affecting 12 million people per year with almost 310 million people at risk. Recently, the WHO has declared leishmaniasis a Category I Neglected Tropical Disease. Leishmaniasis has a range of clinical manifestations, from self-healing skin lesions to hepatomegaly to fatality. The first-line chemotherapies used to treat leishmaniasis are intravenous pentavalent antimonials; however, these drugs are highly toxic. Oral treatment options such as paromomycin and miltefosine have been used more as incidences of disease relapse and drug resistance to antimonials develop, emphasizing the importance of identifying new chemotherapies. We developed a novel, target—free fluorometric high-throughput screen (HTS), with an average Z-score of 0.73 +/- 0.13, to identify small molecules with anti-leishmanial activity. Screening of 10,000 small molecules from the ChemBridge DIVERset-EXPTM library cassette #5 yielded 210 compounds that killed 80 percent of parasites, resulting in a hit rate of 2.1 percent. One hundred nine (109) molecular scaffolds were represented within the hit compounds; one scaffold that exhibits potent anti-leishmanial activity was 1,4-diaryl-pyrazolo-pyridinone (1,4-DAPP). A total of 27 novel 1,4-DAPP compounds were synthesized and anti-leishmanial efficacy and host cell toxicity was determined using L. donovani mCherry expressing amastigotes and THP-1 macrophages; successful drug treatment was considered when the IC50 value was less than 10μM and the CC50 value was greater than 50μM. Additional pharmacokinetic analyses of a potent 1,4-DAPP compound identified in the HTS were conducted. Future studies include in vitro and in vivo characterization of these novel compounds.

Investigation of a Series of 1,4-diaryl-pyrazolo-pyridinones as Anti-Leishmanial Agents

Hannah N. Corman[1], Douglas A. Shoue[1], Bruce J. Melancon[2], Mary Ann McDowell[1]

[1]Eck Institute for Global Health, University of Notre Dame, Notre Dame IN

[2]Warren Center for Drug Discovery and Development, University of Notre Dame, Notre Dame IN

IMPROVING HEALTH THROUGH RESEARCH

indianactsi.org

ABSTRACT

Leishmaniasis is a grouping of diseases caused by the protozoan parasites *Leishmania spp.*, affecting 12 million people per year with almost 310 million people at risk. Recently, the WHO has declared leishmaniasis a Category I Neglected Tropical Disease. Leishmaniasis has a range of clinical manifestations, from self-healing skin lesions to hepatomegaly to fatality. The first-line chemotherapies used to treat leishmaniasis are intravenous pentavalent antimonials; however, these drugs are highly toxic. Oral treatment options such as paromomycin and miltefosine have been used more as incidences of disease relapse and drug resistance to antimonials develop, emphasizing the importance of identifying new chemotherapies. We developed a novel, target—free fluorometric high-throughput screen (HTS), with an average Z-score of 0.73 +/- 0.13, to identify small molecules with anti-leishmanial activity. Screening of 10,000 small molecules from the ChemBridge DIVERset-EXP™ library cassette #5 yielded 210 compounds that killed 80 percent of parasites, resulting in a hit rate of 2.1 percent. One hundred nine (109) molecular scaffolds were represented within the hit compounds; one scaffold that exhibits potent anti-leishmanial activity was 1,4-diaryl-pyrazolo-pyridinone (1,4-DAPP). A total of 27 novel 1,4-DAPP compounds were synthesized and anti-leishmanial efficacy and host cell toxicity was determined using *L. donovani* mCherry expressing amastigotes and THP-1 macrophages; successful drug treatment was considered when the IC_{50} value was less than 10μM and the CC_{50} value was greater than 50μM. Additional pharmacokinetic analyses of a potent 1,4-DAPP compound identified in the HTS were conducted. Future studies include *in vitro* and *in vivo* characterization of these novel compounds.

BACKGROUND

Leishmania spp.

- Obligate intracellular protozoan parasite
- Over 20 species are pathogenic to humans

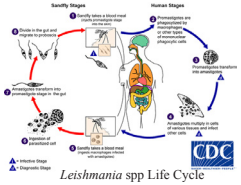

Leishmania spp Life Cycle

Leishmaniasis

- Vector borne parasitic disease
- Affects 12 million people per year
  - 300 million people at risk of infection
- Endemic to South America, Africa, and Eastern Asia
- Treatments include pentavalent antimonials and miltefosine
- Current treatments are highly toxic, expensive, or difficult to administer

Cutaneous

Visceral

This project was funded in part, with support from the Indiana Clinical and Translational Sciences Institute funded, in part by Award Number UL1TR002529 from the National Institutes of Health, National Center for Advancing Translational Sciences, Clinical and Translational Sciences Award. This project was also funded, in part, with support from the University of Notre Dame Eck Institute for Global Health.

In addition, we thank Dr. Mayland Chang and her lab members for their assistance and expertise and the scientists in the Warren Center for Drug Discovery and Development. We also thank the University of Notre Dame CBBI Fellowship Program and CTSI Predoctoral Fellowship.

1,4-DAPP COMPOUNDS

Table 1: Results from high-throughput screen of DIVERset-EXP™ library (cassette #5).

Total compounds present in library	10,000
Effectiveness > 80%	210
Effectiveness > 90%	116
Effectiveness = 50uM Miltefosine	61
# scaffolds (1 compound)	76
# enriched scaffolds (2+ compounds)	33

Figure 1: 1,4-diaryl-pyrazolo-pyridinone (1,4-DAPP) structures and SAR substitution patterns. A. 1,4-DAPP general structure and SAR substitution patterns **B**. Synthesis scheme

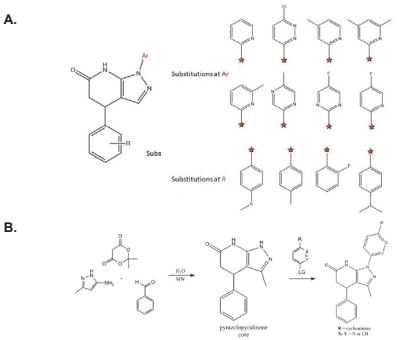

IN VITRO CHARACTERIZATION

Table 2. Secondary screening summary. SI = CC_{50}/IC_{50}. IC_{50} values are for *L. donovani*.

	THP-1	Axenic Amastigotes		Intracellular Amastigotes	
Compound	CC_{50} (μM)	IC_{50} (μM)	SI	IC_{50} (μM)	SI
Miltefosine	28.92	3.34	8.66	1.87	15.47
9279817	>50	3.56	≥14.04	2.28	≥21.97
4127	>50	5.115	≥9.78		
5618	>50	9.897	≥5.05		
6003	>50	10.16	≥4.92		
6004	>50	10.23	≥4.89		
6005	>50	9.675	≥5.17		
6007	>50	14.38	≥3.48		
6008	>50	7.992	≥6.26		
6009	>50	6.149	≥8.13		
6012	>50	20.76	≥2.41		
6013	>50	10.72	≥4.66		
6016	>50	10.48	≥4.77		
6017	>50	11.43	≥4.37		
6026	>50	9.174	≥5.45		
6027	>50	5.423	≥9.22		
6034	>50	6.947	≥7.20		
6035	>50	9.854	≥5.07		
6053	>50	5.651	≥8.85		
6054	>50	9.017	≥5.55		
6064	>50	8.596	≥5.82		
6067	>50	4.661	≥10.73		
6074	>50	32.27	≥1.55		
6095	>50	5.93	≥8.43		
6103	>50	6.545	≥7.64		
6104	>50	15.79	≥3.17		
6145	>50	11.54	≥4.33		
G-17	>50	1.2	≥41.67	5.31	≥9.42
G-18-1	>50	1.3	≥38.46	5.44	≥9.19
G-18-2	>50	1.8	≥27.78	8.65	≥5.78

PHARMACOKINETICS

Figure 2. Plasma concentration-time curve of compound #9279817 after a single intravenous dose at 2mg/kg in female C57BL/6J mice.

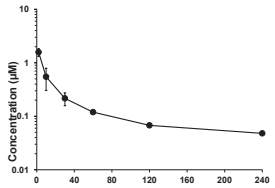

Time (min)	Concentration (μM.min)
2	1.570 ± 0.264
10	0.547 ± 0.243
30	0.210 ± 0.059
60	0.120 ± 0.0013
120	0.068 ± 0.0010
240	0.048 ± 0.0012
AUC_{0-240}	33.7 μM.min
C_0	2.33 μM
$t_{1/2\alpha}$	9.96 min
$t_{1/2\beta}$	99.0 min
Vd	1093 mL/kg
CL	156 mL/min/kg

METABOLITE IDENTIFICATION

Figure 3. Identification of the metabolite (M1) of compound #9279817. **A**. *In vitro* metabolic stability. #9279817 was incubated with rat liver microsomes. Top: analysis of the incubation at time 0. Bottom: analysis of the incubation at time 10 minutes. **B.** Identification of M1 by MS/MS. Top: MS/MS spectrum of compound #9279817; MH+ is at m/z 380. Bottom: MS/MS spectrum of M1; MH+ is at m/z 396.

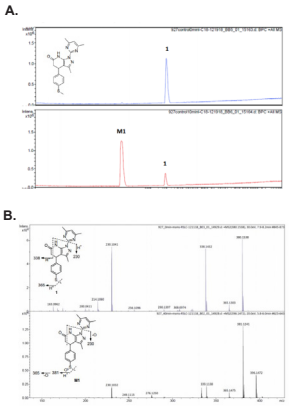

IN VIVO CUTANEOUS MODEL

Figure 4. Balb/c mice were inoculated with *L. major* mCherry promastigotes (10^6) in a footpad. After 14 days, fluorescence values as a proxy for parasite load were obtained using an IVIS Lumina system (day 0). The mice were then treated with antimony(III) tartrate (5 doses/week), #9213357 (5 doses/week), #6666551 (5 doses/week), #9270128 (5 doses/week), and #9243327 (5 doses/week) over a 12-day period. All doses were 30μl intralesional injections of aqueous solutions (0.015 μg/kg). **A.** Representative images shown. The fluorescence intensity scale bar applies to all images and is given in arbitrary units. **B.** Quantification of IVIS Lumina images. Two-way ANOVA with Bonferroni post-hoc analysis was conducted. Differences were regarded as extremely significant when p<0.0001 (*) compared with the Antimony treatment and p<0.0001 (†) compared to the Day 0 control.

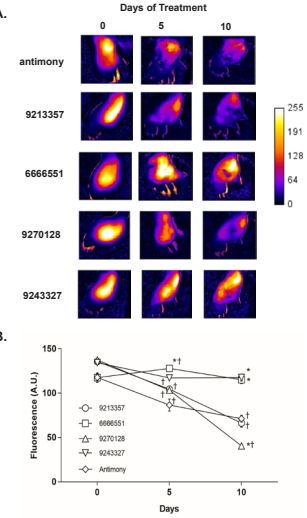

IN VIVO VISCERAL MODEL

Figure 5. VL mouse model. In vivo imaging of mCherry *L. donovani* amastigotes. Briefly, 10^6 metacyclic parasites were injected i.v. in the tail of female Balb/c mice (n=4). Parasite fluorescence was monitored 4 and 8 weeks post-infection (p.i.) in an IVIS Lumina system, using a specific mCherry filter. A representative image is shown. Spleens were photographed and parasite loads calculated by microscopic counting after tissue homogenization.

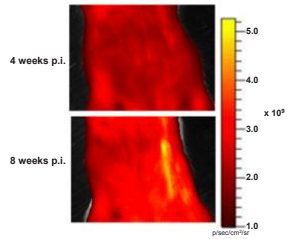

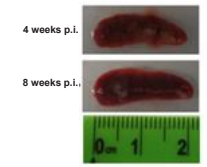

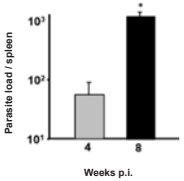

SUMMARY

- Only one compound (#6067) had an IC_{50} value less than 5μM
- Preliminary structure-activity relationship (SAR) analyses suggest an importance for a methyl in the 4-position of the northern aryl ring
  - Of the 15 compounds with IC_{50} values less than 10μM, 6 contained a methyl group in this position
- Compound clearance was almost twice the rate of hepatic blood flow, indicating the compound is rapidly cleared
- Compound distribution was relatively high, indicating the compound distribution to tissue
- MS/MS results suggest S on compound 9279817 is the likely spot for metabolism

FUTURE EXPERIMENTS

- Complete characterize *in vitro* activity of compounds against intracellular amastigotes
- Synthesis of metabolite M1 and *in vitro* characterization
- Determine metabolic stability of G-17, G-18-1, and G-18-2 using rat liver microsomes
- Complete in vivo characterization in CL model of G-17, G-18-1, and G-18-2
- Complete in vivo characterization in VL model of G-17, G-18-1, and G-18-2
- Develop compound-resistant parasite lines to compound 9279817
  - Determine in vitro efficacy after 10x IC50 value resistance is reached
  - Remove drug pressure for 1 month and 4 months to check if resistance is maintained

DETERMINANTS OF ANTIGENICITY IN TUMOR NEOEPITOPES FOR THE DEVELOPMENT OF PERSONALIZED/MULTIPLE PEPTIDE VACCINES

Grant Keller, Graduate Student, University of Notre Dame

Lauren Davancaze, University of Notre Dame

Alyssa, Arbuiso, University of Notre Dame

Hakimeh, Ebrahimi-Nik, University of Connecticut School of Medicine

Vaccines incorporating mutant tumor peptides, or "neoantigens," represent a low-cost, broadly applicable type of immunotherapy which can sensitize the immune system to tumors, break tolerance, and confer long-lasting immunologic memory with fine specificity.

Predicting which candidate neoantigens will likely be immunogenic is imprecise, which limits applicability in treating spontaneous tumors. Structural features of peptide-MHC proteins can be used to predicted immunogenicity better than many tools but is in its infancy and has only been tested on HLA-A*02:01 nonameric peptides. In this study, we identified a group of mutant peptides presented by class I MHC in a non-spontaneous murine cancer model and rationalized the observed immunogenicity with molecular modeling experiments, as predicted IC50 alone did not explain reactivity. After solving the crystal structure of one pair of neoantigens, we propose ways to improve peptide-MHC model selection.

Determinants of Antigenicity in Tumor Neoepitopes for the Development of Personalized/Multiple Peptide Vaccines

Keller G[1], Davancaze L[1], Arbuiso A[1], Ebrahimi-Nik H[2], Srivastava P[2], Baker B[2].

1. Dept. of Chemistry & Biochemistry and Harper Cancer Research Institute, University of Notre Dame. 2. Dept. of Immunology, University of Connecticut School of Medicine.

Abstract

Vaccines incorporating mutant tumor peptides, or "neoantigens," represent a low-cost, broadly applicable type of immunotherapy which can sensitize the immune system to tumors, break tolerance, and confer long-lasting immunologic memory with fine specificity.

Predicting which candidate neoantigens will likely be immunogenic is imprecise, which limits applicability in treating spontaneous tumors. Structural features of peptide-MHC proteins can be used to predicted immunogenicity better than many tools but is in its infancy and has only been tested on HLA-A*02:01 nonameric peptides.

In this study, we identified a group of mutant peptides presented by class I MHC in a non-spontaneous murine cancer model and rationalized the observed immunogenicity with molecular modeling experiments, as predicted IC_{50} alone did not explain reactivity. After solving the crystal structure of one pair of neoantigens, we propose ways to improve peptide-MHC model selection.

MHC binding does not (always) predict immunological outcome

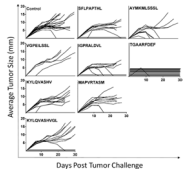

Name	Allele	Sequence (WT/NEO)	WT IC_{50} (nM)	Mutant IC_{50} (nM)	Tumor Rejection	T cell response
C2-1	H-2D^d	VGPEILSS(R/L)	9627.31	1451.3	-	++
C3-1	H-2D^d	TGAA(S/R)PDEF	3265.23	499.0	+++++	++
C8-1	H-2D^d	IGPR(A/L)VDVL	237.19	156.6	+++	+
C10-1	H-2K^d	AY(L/M)KMLSSSL	35.39	22.1	+++	-
C11-1	H-2D^d	MAPVRTAS(L/M)	7818.7	13767.3	++	N/A
C12-1	H-2K^d	SFLPAPT(Q/H)L	104.32	61.1	++	-
C19-1	H-2K^d	KY(R/L)QVASHVGL	189.47	40.1	+	++
C19-3	H-2K^d	KY(R/L)QVASHV	21.97	9.4	-	-

Immunization with BMDCs primed with tumor neoepitopes resulted in variable tumor rejection and CD8$^+$ T cell response irrespective of improvement in predicted MHC affinity upon mutation.

Antigen structure informs T cell response

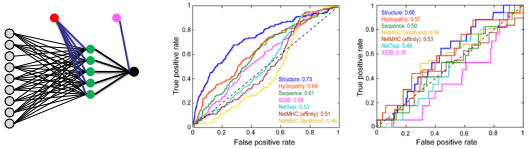

Previously, we developed an artificial neural network to predict immunogenicity of HLA-A*02:01 9mer peptides based on structure alone, which outperformed other prediction methods.

C3-1 crystal structures reveal flaws, strengths in modeling

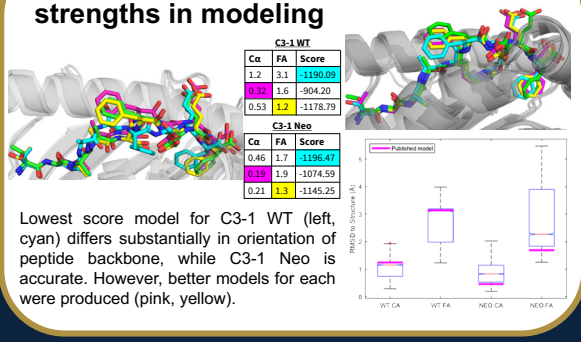

C3-1 WT		
Cα	FA	Score
1.2	3.1	-1190.09
0.32	1.6	-904.20
0.53	1.2	-1178.79

C3-1 Neo		
Cα	FA	Score
0.46	1.7	-1196.47
0.19	1.9	-1074.59
0.21	1.3	-1145.25

Lowest score model for C3-1 WT (left, cyan) differs substantially in orientation of peptide backbone, while C3-1 Neo is accurate. However, better models for each were produced (pink, yellow).

Score function components describe structure better than total

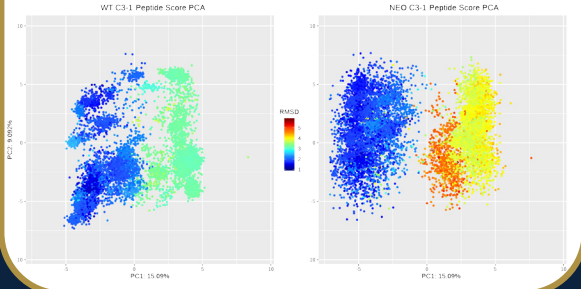

Support vector regression models improve accuracy vs. total score

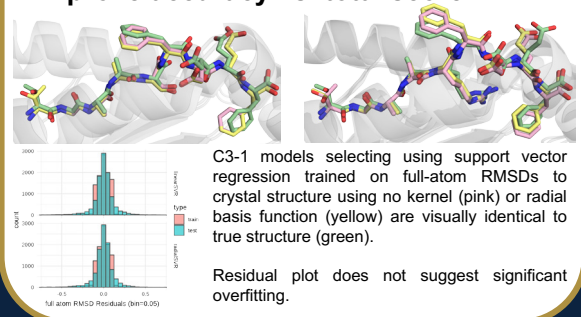

C3-1 models selecting using support vector regression trained on full-atom RMSDs to crystal structure using no kernel (pink) or radial basis function (yellow) are visually identical to true structure (green).

Residual plot does not suggest significant overfitting.

SVR-based structural model selection appears generally applicable

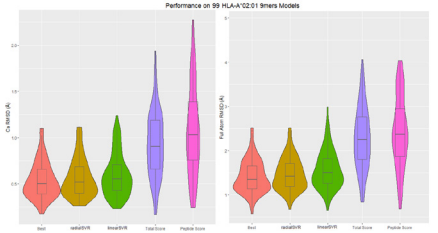

A similar model selection method was applied to all 99 structures of nonameric peptides presented by HLA-A*02:01 and outperformed selection by score. Performance by full-atom RMSD approached optimality for SVR employing a radial basis function kernel.

Conclusions and Future Directions

- peptide-MHC structure can predict immunogenicity
- model is accurate, but selection is poor
- per-residue energy can be fit to improve selection for some alleles

Moving forward we will:

- Validate on newly-solved structures.
- Investigate if this method is allele-specific, length-specific, or generalizable (with context).

Citations

1. Ebrahimi-Nik H, Michaux J, Corwin WL, *et al.* (2019). **Mass spectrometry driven exploration reveals nuances of neoepitope-driven tumor rejection**. *JCI Insight*.
2. Riley TP, Keller GLJ, Smith AR, *et al.* (2019) **Structure-Based Prediction of Neoantigen Immunogenicity**. *Frontiers in Immunology*.
3. Chaudhury S, Lyskov S, Gray JJ. (2010). **PyRosetta: a script-based interface for implementing molecular modeling algorithms using Rosetta**. *Bioinformatics*.

This project was supported, in part, with support from the Indiana Clinical and Translational Sciences Institute funded, in part by Grant Number TL1TR002531 from the National Institutes of Health, National Center for Advancing Translational Sciences, Clinical and Translational Sciences Award.

INSIGHTS FROM AN IN VITRO DERIVED T CELL RECEPTOR

Jesus Alonso, Postdoctoral Research Associate, University of Notre Dame

Nishant K. Singh, Ragon Institute, Harvard and the Massachusets Institute of Technology

David Kranz, Department of Biochemistry, University of Illinois Urbana-Champaign

Brian Evavold, Department of Pathology, University of Utah School of Medicine

Brian M. Baker, Department of Chemistry and Biochemistry, University of Notre Dame

Heterodimeric alpha-beta T cell receptors (TCRs) play a key role in cell-mediated immune responses of adaptive immunity. T cells continuously probe peptides presented by major histocompatibility complex (MHC) found on the cell surface. T cell activation initiates through the binding of antigenic peptides on MHCs. Yeast display technology has proven an effective way to gain insight into the underpinnings of peptide-MHC specificity enabling the switching of TCR affinity and specificity to unrelated antigens through directed evolution. Interestingly, in vitro directed evolution also generates mutants that lose peptide specificity. Here, we provide further detail of one of these cross-reactive TCRs, S3-4, which binds tightly but with a highly unusual geometry. Despite binding with an affinity that is characteristic of a strong agonist, S3-4's odd binding geometry does not support T cell signaling. Further investigation with functional experiments and 2D kinetics shows that lack of signaling by S3-4 is ultimately attributable to the TCR's inability to reach ligand. Although S3-4 is an example from a constrained system generated outside the bounds of usual immune function, our results show how unusual binding can influence T cell function and further demonstrate how divergences between 3D and 2D binding parameters can emerge.

Insights from an *in vitro* derived T Cell Receptor

Nishant K. Singh[2], Jesus A. Alonso[1], David Kranz[3], Brian Evavold[4], and Brian M. Baker[1]

[1]Department of Chemistry and Biochemistry, Harper Cancer Institute, University of Notre Dame, [2]Ragon Institute of Massachusetts General Hospital, Harvard University and MIT, [3]Department of Biochemistry, University of Illinois Urbana-Champaign, [4]Department of Pathology, University of Utah School of Medicine

ABSTRACT Heterodimeric αβ T cell receptors (TCRs) play a key role in cell-mediated immune responses of adaptive immunity. T cells continuously probe peptides presented by major histocompatibility complex (MHC) found on the cell surface. Yeast display technology has proven an effective way to gain insight into the underpinnings of peptide-MHC specificity enabling the switching of TCR affinity and specificity to unrelated antigens through directed evolution. Interestingly, *in vitro* directed evolution also generates mutants that lose peptide specificity. Here, we provide further detail of one of these cross-reactive TCRs, S3-4, which binds tightly but with a highly unusual geometry. Despite binding with an affinity that is characteristic of a strong agonist, S3-4's odd binding geometry does not support T cell signaling. Further investigation with functional experiments and 2D kinetics shows that lack of signaling by S3-4 is ultimately attributable to the TCR's inability to reach ligand. Although S3-4 is an example from a constrained system generated outside the bounds of usual immune function, our results show how unusual binding can influence T cell function and further demonstrate how divergences between 3D and 2D binding parameters can emerge.

Figure 1

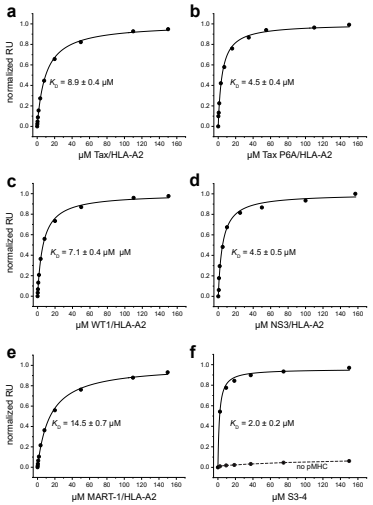

Figure 2

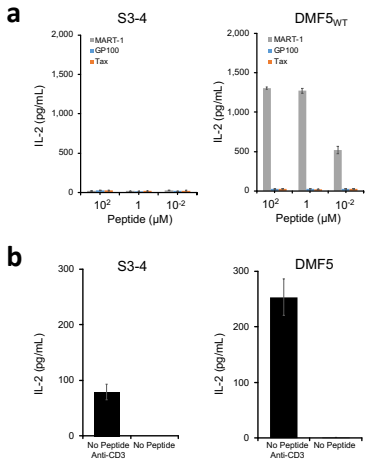

Figure 3

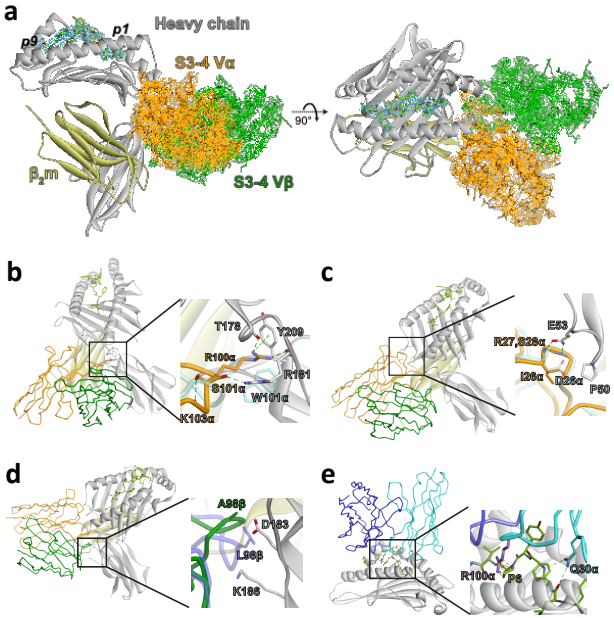

Figure 1. S3-4 binds HLA-A2 in a peptide-independent manner.

Recombinantly expressed S3-4 tested for binding against peptide/HLA-A2 complexes **(a)** Tax/HLA-A2 **(b)** Tax P6A/HLA-A2 **(c)** WT1/HLA-A2 **(d)** NS3/HLA-A2 and **(e)** MART1/HLA-A2 and demonstrating HLA-A2 independent binding. K_D = binding affinity.

Figure 2. Full length S3-4 does not support signaling.

Full length S3-4 was expressed in transduced Jurkat cells and tested for signaling against peptide-pulsed antigen presenting cells (T2). Although S3-4 shows no signaling against MART1, gp100 or Tax **(a)**, it did show signaling when primed with the anti-CD3 antibody OKT3 **(b)**. MART1 is the DMF5 TCR cognate antigen.

Figure 3. S3-4 binds HLA-A2 on the side.

(a) Crystal structure of S3-4 bound to Tax/HLA-A2 reveals that S3-4 binds on the side of the HLA-A2. **(b - e)** Illustration of how the six S3-4 mutations altered binding of the TCR to HLA-A2. In general, they act by introducing new interactions with the side of HLA-A2 as well as eliminating steric or electronic clashes which would occur with the new positioning.

Figure 4

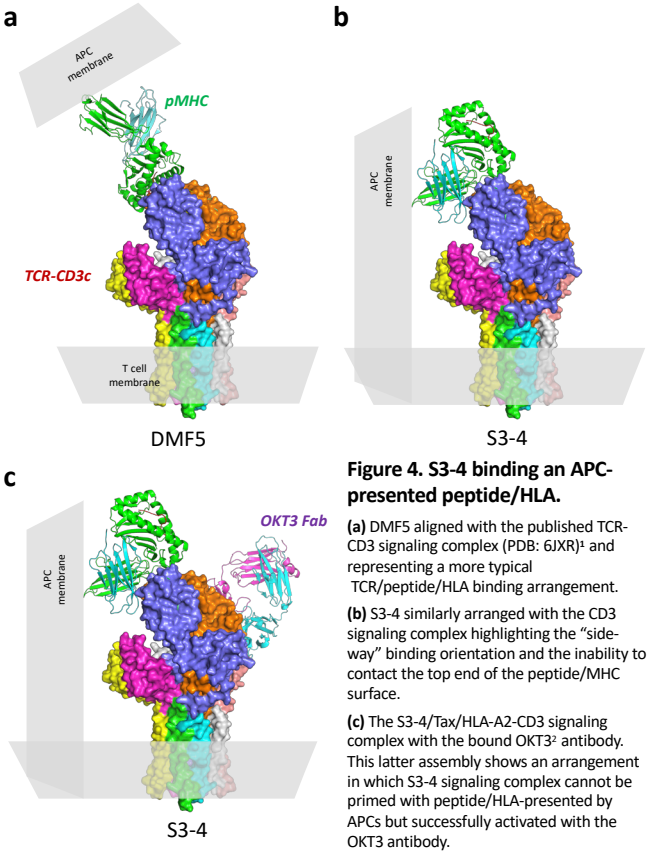

Figure 4. S3-4 binding an APC-presented peptide/HLA.

(a) DMF5 aligned with the published TCR-CD3 signaling complex (PDB: 6JXR)[1] and representing a more typical TCR/peptide/HLA binding arrangement.

(b) S3-4 similarly arranged with the CD3 signaling complex highlighting the "side-way" binding orientation and the inability to contact the top end of the peptide/MHC surface.

(c) The S3-4/Tax/HLA-A2-CD3 signaling complex with the bound OKT3[2] antibody. This latter assembly shows an arrangement in which S3-4 signaling complex cannot be primed with peptide/HLA-presented by APCs but successfully activated with the OKT3 antibody.

REFERENCES

1. Zheng, L. et al., *Nature*. 2019 September 11
2. Kjer-Nielsen, L. et al., *P.N.A.S.* 2004. May 25

INTERROGATING THE CLINICALLY-RELEVANT T CELL RECEPTOR TIL1383I

Aaron Rosenberg, Graduate Student,
University of Notre Dame

Immunotherapy using gene-modified T cells is emerging as a new option in cancer treatment. Early studies using adoptive transfer of T cells engineered to express T cell receptors specific to tumor antigens have shown promising results in both solid and hematological cancers. A recent clinical trial of adoptive T cell therapy utilizing the TIL1383i TCR to treat stage IV melanoma has shown promising results. However, there are ongoing questions about TCR-engineered T cells, most notably whether efficacy can be enhanced without increasing risk. Here, I plan to biochemically and functionally interrogate the TIL1383i TCR. I will use deep mutational scanning, which provides single-amino acid resolution of the physical determinants of specificity and affinity across an entire protein interface. In conjunction with our existing, unpublished crystallographic structure of TIL1383i, this work will allow us to better understand the immunological behavior of TIL1383i and potentially generate improved variants for follow-on clinical work.

Interrogating the clinically-relevant T cell receptor TIL 1383i

Aaron Rosenberg[1], Michael Nishimura[2], Brian M. Baker[1]
Department of Chemistry and Biochemistry[1], Harper Cancer Research Institute, University of Notre Dame, Notre Dame, IN
Loyola University Medical Center, Maywood, IL[2]

Introduction

T cell-based immunotherapy relies on the interaction between a therapeutic T cell receptor (TCR) and a target peptide presented by a major histocompatibility complex protein presented on a tumor cell surface (pMHC). TCRs bind pMHC complexes using six complementarity determining region (CDR) loops.[1] The strength and specificity of the interaction is influenced not only by the CDR residues directly contacting the pMHC, but also those further away in the TCR framework region in what has been termed the "second shell." Modification of second shell residues has been shown to allow TCR affinity and potency to be improved while preserving antigen specificity.[2, 3]

Figure 1: Peptide MHC bound by a heterodimeric αβ TCR. The TCR is positioned above the pMHC with the α chain in purple and the β chain in blue. The MHC is composed of the HLA subunit (gray) and the β_2m subunit (green). The peptide (orange) is positioned between the two α helices of the MHC. PDB: 3QDG

It is recognized that increasing T cell potency is necessary for stronger anti-tumor immunity. Unfortunately, traditional ways of modulating TCR affinity have been associated with increasing the risk of off-target toxicity by weakening antigen specificity.[4-6] I propose to utilize deep mutational scanning to construct a detailed map of how the residues in the CDR loops and the second shell can be mutated to improve TCR function. Deep mutational scanning is a recently described technique for rapidly assessing the impact of multiple mutations throughout a protein.[7] Recent work has shown how deep mutational scanning can be used to generate novel TCR variants with enhanced affinity.[3, 6] In conjunction with crystal structures of the TCR bound to the pMHC complex, the deep mutational scanning data will allow me to assess residues in the CDR loops and second shell that contribute to binding properties.

Single Chain TCR

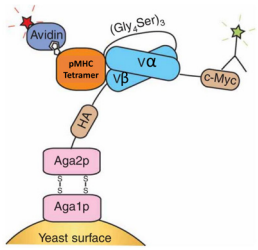

Modified from: Chao, 2006, Isolating and engineering human antibodies using yeast surface display

Figure 2: Single Chain TCR Construct for Yeast Display. The use of yeast in conjunction with the single chain construct enables for surface display of TCRs. The utilization of this construct also allows for multiple staining options including anti-cMyc, anti-HA, and pMHC tetramers.

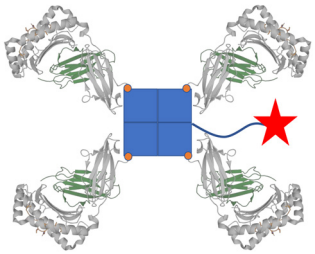

Figure 3: Cartoon Representation of pMHC Tetramer. The blue squares represent the four subunits of the streptavidin core connected to the fluorophore represented by the red star. The four pMHC molecules, shown in grey and green, are bound to the streptavidin through the addition of biotin (orange circles) of the C-terminus of the MHC molecules.

Nicking Saturation Mutagenesis

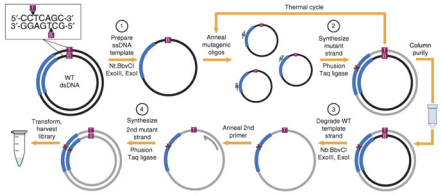

Wrenbeck, 2016, Plasmid-based one-pot saturation mutagenesis

Figure 4: Nicking Saturation Mutagenesis (NSM) Overview. Nicking saturation mutagenesis allows for high efficiency, one pot saturation mutagenesis reactions for deep mutational scanning.

868-Z11 Single Chain TCR

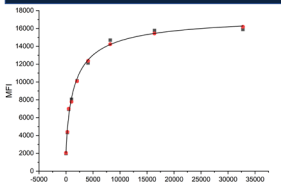

Figure 5: Single Chain 868-Z11 WT TCR Yeast Display Titration. Wild type 868-Z11 TCR was displayed on the surface of yeast. HLA-A2/SL9 pMHC tetramer was titrated between 256 pM to 32.8 nM. The MFI data was graphed and used to determine the K_D of the WT 868-Z11 TCR to the HLA-A2/SL9 tetramer. The K_D was determined to be 1.7 ± 0.6 nM.

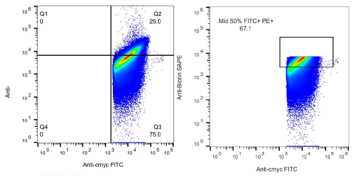

Figure 6: Representative Sort of 868-Z11 TCR library with HLA-A2/SL9 pMHC Tetramer. 868-Z11 saturation mutagenesis libraries were sorted using anti-cMyc FITC and HLA-A2/SL9 pMHC tetramer conjugated to PE. Two separate populations were collected: the top 25% of the double positive cells and the next 50% of the double positive population.

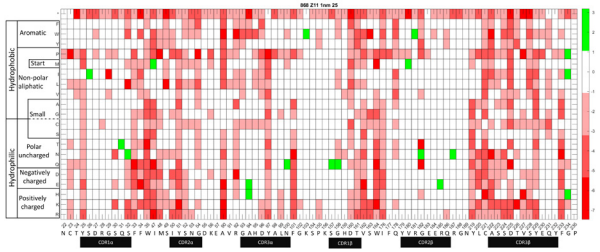

Figure 7: Heatmap of fitness values of 868-Z11 TCR library sorted with SL9 MHC Tetramer. Fitness values plotted as a heatmap for all mutations in 868-Z11 libraries based upon deep sequencing of the top 25% population sorted at 1 nM. Green represents increased fitness due to mutation whereas red represents a decrease in fitness due to mutation. Black bars indicate the CDR loops. The WT sequences is shown below the residue number.

Positive Fitness Mutations

R187N	3.19
A94H	2.19
G234P	1.96
G182N	1.85
G234H	1.85

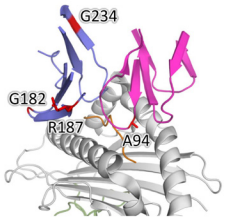

Figure 8: Top 5 Positively Enriched Residues. The top 5 most positive fitness mutations are highlighted in red on the structure. The fitness values are calculated from the $\log_2$ enrichment values normalized by WT enrichment and are provided in the table above. The structure is modified from PDB: 5NME.

Negative Fitness Mutations

A90E	-7.47
F101N	-7.10
V227P	-6.78
R92W	-6.63
I47R	-6.59
R92D	-6.59

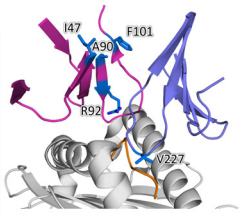

Figure 9: Top 6 Most Negatively Enriched Residues. The top 6 most negative fitness mutations are highlighted in blue on the structure. The fitness values are calculated from the $\log_2$ enrichment values normalized by WT enrichment and are provided in the adjacent table. The structure is modified from PDB: 5NME.

TIL 1383i TCR

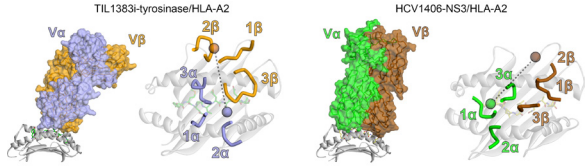

Figure 10: Binding mode of TIL 1383i and HCV1406 pMHC Complexes. TIL 1383i is shown in complex with HLA-A2/Tyrosinase in blue and orange. HVC 1406 is shown in complex with HLA-A2/NS3 in green and brown. In the adjacent top down view of the pMHC, the spheres represent the center of masses for each of the respective variable domains of the TCRs in addition to the CDR loops.

- TIL 1383i is a clinically relevant TCR that has been used with some success in phase I clinical trials for treatment of stage IV melanoma patients.
- TIL 1383i has an unusual binding mode when compared to other class I restricted TCRs.
- TIL 1383i was isolated from a CD4+ T cell but recognizes a class I pMHC (HLA-A2/Tyrosinase).
- Aim: Interrogate the CRD loops and second shell for TIL 1383i with single amino acid resolution to provide a comprehensive understanding of the drivers of affinity and specificity across the TCR pMHC interface.

Future Goals

- Utilize fitness data in conjunction with crystal data to identify mutations in which to further interrogate their role in the modulation of affinity specificity.
- Characterize mutations located in the TCR pMHC binding interface and the second shell. Determine alterations in binding affinity and specificity through SPR and combinatorial peptide library screens.
- Interrogate the clinically relevant TCR TIL 1383i utilizing the same methods and lesson learned.

Reference

1. Rossjohn, J.; Gras, S.; Miles, J. J.; Turner, S. J.; Godfrey, D. I.; McCluskey, J., T cell antigen receptor recognition of antigen-presenting molecules. *Annu Rev Immunol* **2015,** *33*, 169-200.
2. Sharma, P.; Kranz, D. M., Subtle changes at the variable domain interface of the T-cell receptor can strongly increase affinity. *J Biol Chem* **2018,** *293* (5), 1820-1834.
3. Harris, D. T.; Wang, N.; Riley, T. P.; Anderson, S. D.; Singh, N. K.; Procko, E.; Baker, B. M.; Kranz, D. M., Deep Mutational Scans as a Guide to Engineering High Affinity T Cell Receptor Interactions with Peptide-bound Major Histocompatibility Complex. *J Biol Chem* **2016,** *291* (47), 24566-24578.
Cameron, B. J.; Gerry, A. B.; Dukes, J.; Harper, J. V.; Kannan, V.; Bianchi, F. C.; Grand, F.; Brewer, J. E.; Gupta, M.; Plesa, G.; Bossi, G.; Vuidepot, A.; Powlesland, A. S.; Legg, A.; Adams, K. J.; Bennett, A. D.; Pumphrey, N. J.; Williams, D. D.; Binder-Scholl, G.; Kulikovskaya, I.; Levine, B. L.; Riley, J. L.; Varela-Rohena, A.; Stadtmauer, E. A.; Rapoport, A. P.; Linette, G. P.; June, C. H.; Hassan, N. J.; Kalos, M.; Jakobsen, B. K., Identification of a Titin-derived HLA-A1-presented peptide as a cross-reactive target for engineered MAGE A3-directed T cells. *Sci Transl Med* **2013,** *5* (197), 197ra103.
4. Linette, G. P.; Stadtmauer, E. A.; Maus, M. V.; Rapoport, A. P.; Levine, B. L.; Emery, L.; Litzky, L.; Bagg, A.; Carreno, B. M.; Cimino, P. J.; Binder-Scholl, G. K.; Smethurst, D. P.; Gerry, A. B.; Pumphrey, N. J.; Bennett, A. D.; Brewer, J. E.; Dukes, J.; Harper, J.; Tayton-Martin, H. K.; Jakobsen, B. K.; Hassan, N. J.; Kalos, M.; June, C. H., Cardiovascular toxicity and titin cross-reactivity of affinity-enhanced T cells in myeloma and melanoma. *Blood* **2013,** *122* (6), 863-71.
5. Morgan, R. A.; Chinnasamy, N.; Abate-Daga, D.; Gros, A.; Robbins, P. F.; Zheng, Z.; Dudley, M. E.; Feldman, S. A.; Yang, J. C.; Sherry, R. M.; Phan, G. Q.; Hughes, M. S.; Kammula, U. S.; Miller, A. D.; Hessman, C. J.; Stewart, A. A.; Restifo, N. P.; Quezado, M. M.; Alimchandani, M.; Rosenberg, A. Z.; Nath, A.; Wang, T.; Bielekova, B.; Wuest, S. C.; Akula, N.; McMahon, F. J.; Wilde, S.; Mosetter, B.; Schendel, D. J.; Laurencot, C. M.; Rosenberg, S. A., Cancer regression and neurological toxicity following anti-MAGE-A3 TCR gene therapy. *J Immunother* **2013,** *36* (2), 133-51.
6. Harris, D. T.; Singh, N. K.; Cai, Q.; Smith, S. N.; Vander Kooi, C.; Procko, E.; Kranz, D. M.; Baker, B. M., An Engineered Switch in T Cell Receptor Specificity Leads to an Unusual but Functional Binding Geometry. *Structure* **2016,** *24* (7), 1142-1154.
7. Araya, C. L.; Fowler, D. M., Deep mutational scanning: assessing protein function on a massive scale. *Trends Biotechnol* **2011,** *29* (9), 435-42.